NUMERICAL ANALYSIS OF THE VOLTAGE-CLAMP TECHNIQUE APPLIED TO FROG NEUROMUSCULAR JUNCTIONS

MIGUEL E. TORRES, CARLOS SEVCIK, AND VALENTÍN PARTHE
Laboratory of Cellular Neuropharmacology and Laboratory of Neurophysiology "Santiago Ramón y Cajal", Centro de Biofísica y Bioquímica, Instituto Venezolano de Investigaciones Científicas, Apariado 1827, Caracas 1010 A, Venezuela

ABSTRACT The nonlinear cable equation was solved numerically by means of an implicit procedure. The correlation between end-plate length and fiber diameter was determined in frog (*Rana pipiens*) sartorius muscles stained with gold chloride (Löwit, 1875). The diameter of the fibers stained by the Löwit method was 80 (74–85) μm (median and its 95% confidence interval for 52 fibers), the length of the end plates in the same fibers was 382 (353–417) μm. The fibers simulated were 80 μm in diameter. To solve the equation the muscle fibers were represented by 500 segments 20 μm long, and the equation was solved in steps of 10 μs; a double exponential function was incorporated to the first seven segments to represent the neuromuscular junction. The potential of the first segment of the cable was set to the clamping level and the membrane potential of the remaining segments calculated. The current needed to hold the first segment was estimated by adding the current flowing through the first segment to the current flowing from it to the second segment. Our results indicate that the lack of space clamp in the point voltage-clamp studies of the frog neuromuscular junction introduces serious errors in the estimates of the end-plate conductance value, the kinetics of the conductance changes, and the reversal potential of the end-plate currents. The possibility of an efficient voltage-clamp technique is also explored. Our calculations suggest that the study of end-plate current and conductance is possible with little error if the end-plate potential is controlled at both ends of the synaptic area simultaneously.

INTRODUCTION

An understanding of the neuromuscular transmission of impulses is of great importance for neurophysiology. The success of the voltage-clamp approach to analyze and reconstruct the electrical activity in squid nerves (Hodgkin et al., 1952; Hodgkin and Huxley, 1952 *a–d*) is responsible for the extensive application of this technique to many other kinds of excitable tissues. Unfortunately, sometimes the experimenters have applied this powerful technique without giving proper consideration to all of the variables involved in the experimental design. It has been shown for example, by Kootsey and Johnson (1972), that this happens in many studies carried out in cardiac muscle.

The voltage-clamp approach was first applied to neuromuscular transmission by Takeuchi and Takeuchi (1959), and was subsequently utilized by a great number of authors. In all these studies the membrane potential is held at a certain level near the center of the end-plate region and, after the current reaches a steady level, the nerve is stimulated or the neurotransmitter is applied by some other means. The difference between the current necessary to hold the point at the desired level (control current) before (basal control current) and during the action of the neurotransmitter is regarded as the current flowing through the end-plate membrane (end-plate current [EPC]).

The purpose of this communication is to analyze the effect of the lack of spatial voltage control on the EPC estimated by means of point voltage clamp. To achieve this, a mathematical function representing the end plate was added to the first seven segments of a nonlinear cable representing a frog muscle fiber. The control current calculated from the cable was compared with the current predicted by the end-plate function under space- and voltage-clamp conditions.

The results indicate that the point voltage-clamp technique is likely to produce values for the EPC that differ from the true EPC in magnitude, kinetics, and in reversal potential. We have also explored the possibility of using a novel technique for voltage clamping the end-plate area. Our calculations suggest that this is possible if the membrane potential is controlled at both ends of the neuromuscular junction simultaneously, perhaps with some kind of double-clamp circuit with four microelectrodes, or by creating an artificial node with sucrose or vaseline gaps at both extremes of the end plate.

METHODS

The dimension of the muscle fibers and the length of the end plates were measured in frog (*Rana pipiens*) sartorius muscles stained with the Löwit (1875) gold chloride method. Pictures of the fibers were taken with a Zeiss photomicroscope (Carl Zeiss, Inc, New York) and measured by comparison with a picture on a micrometer scale at the same magnification. The possible retraction or swelling produced by the staining procedure was estimated by comparing the diameters of these fibers with unstained fibers in normal Ringer solution.

The data in Fig. 11 were obtained by point voltage clamping the foci of the end plates in two frog sartorius muscle fibres. The muscles were treated with ethylene glycol (EG) to uncouple excitation and contraction. The only modifications introduced to the original EG method (Sevcik and Narahashi, 1972) were to remove by dissection most of the connective tissue lining the external phase of the muscle before immersion in EG Ringer, and the addition of heparine (1 USP unit/ml Ringer) to the solution in which the frog legs were immersed during dissection of the muscles, to prevent the formation of fibrin meshes on their surfaces. Glass microelectrodes were pulled from quick-filling capillaries (type GC 120-F-6, Clark Electromedical Instruments, Pangbourne, Reading, England). The microelectrodes were filled with 2 M K-citrate when used to pass current, and with 3 M KCl to record potential. The resistance of the microelectrodes ranged from 8 to 10 MΩ. The control amplifier (type 171, Analog Devices, Norwood, MA) was able to reach 50 V at the output, and was properly tuned for stability reaching a rise time close to 0.5 ms. Three microelectrodes were inserted into a single fiber under a stereomicroscope (M5A, Wild, Heerbrugg, Switzerland). A current-injecting and a voltage-sensing electrode were placed in the end-plate focus, determined as indicated by Takeuchi and Takeuchi (1959). The distance between the tips of these electrodes was not > 40 μm. A third electrode, to record the changes in potential profile, was inserted at ~200 μm from the other two. All the distances were estimated with a micrometer eyepiece calibrated to measure 20 μm per division. The potential at the end-plate focus (V_0) and 200 μm away from it (V_{200}) was measured differentialy with respect to a similar microelectrode placed in the Ringer solution close to the end-plate region. The experimental chamber was grounded through the input of a current-to-voltage converter used to measure the current needed to control the end plate (I_{ep}). The neuromuscular junction was activated by nerve stimulation with a suction electrode. The normal and EG Ringer solution had the same composition used by Sevcik and Narahashi (1972).

The well-known cable function (Hodgkin and Rushton, 1946) was solved numerically by means of the implicit procedure of Crank and Nicholson (1947). To minimize the error from dividing the cable, the solution was obtained by replacing the time and space derivatives by finite differences at the point $[m\delta x, (n + \theta)\,\delta t]$, with

$$\theta = (6\,\delta t/\delta x^2 - 1)/(12\,\delta t/\delta x^2) \qquad (1)$$

as indicated by Forsythe and Wassow (1960), instead of using $\theta = 1/2$. The symbols are m, number of segment; n, number of time step; δx, segment length (cm); δt, time step (ms).

The ionic currents flowing through the sarcolemma were described by a set of expressions similar to the ones formulated by Hodgkin and Huxley (1952*d*) for the squid nerve. These equations were solved with the parameters of Adrian et al. (1970) and modified by Adrian and Peachey (1973). The membrane capacitance (C_m), however, was lumped and set to a value of 4 μF/cm² of surface membrane. The sarcoplasm resistivity was set as 200 Ωcm.

The numerical solution of the cable equation was carried out in steps of 10 μs, over 500 segments 20 μm long. The cable was assumed to be symmetric about the first segment and terminated with infinite resistance (Arispe, 1972). The EPC (mA/cm) were simulated with the following function (end-plate function):

$$i_{ep} = \hat{g}_{ep} \exp(-T/\phi_1) \cdot [1 - \exp(-T/\phi_2)] \cdot (V - E_{ep})/f(\phi) \qquad (2)$$

where $\hat{g}_{ep}$ = maximum end-plate conductance per unit length (1 mS/cm for a fiber of 80 μm in diameter); $\phi_1 = \tau_1 \bar{g}_l/C_m = \tau_1/\tau_m$ (normalized τ_1); $\phi_2 = \tau_2 \bar{g}_l/C_m = \tau_2/\tau_m$ (normalized τ_2); $T = t\bar{g}_l/C_m = t/\tau_m$ (time in normalized time units [NTU]); $\bar{g}_l$ = membrane leakage conductance (0.24 mS/cm²); t = time (ms); V = membrane potential at time = T, plus 95 mV; E_{ep} = reversal potential of the EPC. The normalization function $f(\phi)$ is given by the expressions

$$f(\phi) = \exp(-t^\circ/\phi_1)\,[1 - \exp(-t^\circ/\phi_2)] \qquad (3)$$

and

$$t^\circ = \phi_2 \ln[(\phi_1 + \phi_2)/\phi_2]\,. \qquad (4)$$

The EPC calculated by Eq. 2, was added to the ionic current in segments 1–7 of the cable.

At any time, the control current (mA) may be found with the following equation:

$$I_{vc} = (V_{1,T} - V_{2,T})/(\delta x\, r_i) + I_{gl} + I_{epl} \qquad (5)$$

where $V_{1,T}$ and $V_{2,T}$ are the membrane potentials of the first and second segments, respectively, at time = T; r_i is the resistence per unit length of the sarcoplasm (ohm/cm); I_{gl} is the ionic current flowing through the sarcolemma in the first segment (mA); and I_{epl} is the EPC (mA) in the first segment ($i_{ep}\delta x$).

All the numerical procedures were programmed in Fortran IV. The operations were carried out with double precision (17 digits), initially in a PDP 11/10 computer (Digital Equipment Corp., Maynard, MA) equipped with a 16K word memory. The solution of the complete equations was obtained in a PDP 11/34 computer with 96K word memory. The results were displayed on a graphics terminal (model 4012, Tektronix Inc., Beaverton, Oregon) and a hardcopy unit (model 4631, Tektronix Inc.).

RESULTS

The Measurement of End-plate Length and Muscle Fiber Diameter

Although data on the correlation between the area of the end-plate vs. fiber diameter have been published by Kuno et al. (1971), extensive review of the literature resulted in no quantitative information on the correlation between end-plate length and fiber diameter. Thus these dimensions were measured in sartorius muscles of *Rana pipiens* stained by the gold chloride method of Löwit (1875). Fig. 1 shows three representative end plates stained with this method. Fig. 2 is a plot of end-plate length vs. fiber diameter determined in 52 neuromuscular junctions. The line was fitted by nonparametric lineal regression [Theil procedure, see Hollander and Wolfe (1973) for details of all nonparametric statistical procedures used in this work], its slope and intercept are, respectively, 3.72 (3.20 – 4.22) μm/μm and 95.4 (58.8 – 125.2) μm (medians and their 95% confidence interval, Hodges and Lehmann statistics). The Spearman correlation coefficient (0.537) indicates a highly significant correlation ($P = 4.10^{-5}$). The values of median end-plate length and fiber diameter in the same fibers are 382 (353–417) and 80 (74–85) μm, respectively.

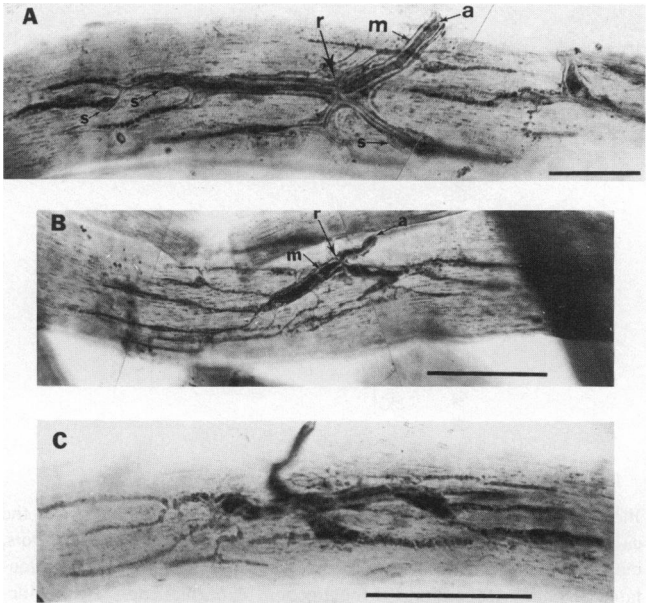

FIGURE 1 Frog neuromuscular junctions. Three different junctions are presented. *A* and *B* are mosaics assembled to compensate for differences in focal plane; the focus of the pictures is set for the nerve terminal, producing a somewhat diffuse appearance of the striation of miofibrils. *a* = axon, *m* = myelin sheath, *r* = node of Ranvier, and *s* = Schwann cell nuclei. Löwit Method was used. Calibration is 50 μm for *A* and 100 μm for *B* and *C*.

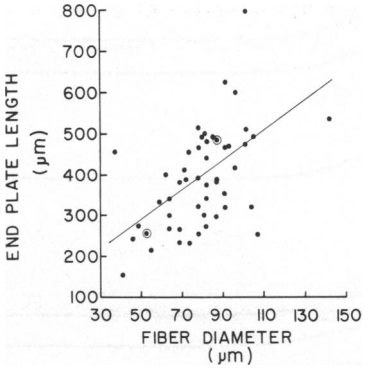

FIGURE 2 Correlation of end-plate length with muscle fiber diameter. The figure presents the end-plate length as function of the diameter in 52 different junctions, both dimentions in micrometers. Concentric circles indicate two points with equal coordinates. The straight lines were calculated by the Theil nonparametric regression, and correspond to the following parameters: slope = 3.72 (3.20, 4.22) μm/μm, intercept = 95.4 (58.8, 125.2) μm, Spearman correlation coefficient = 0.537. The probability that the correlation is not significant is 4.10^{-5}.

The Löwit method produces no significant change in fiber dimensions because the median diameter of 19 unstained fibers in normal Ringer solution was 87 (81–96) μm; the difference is not statistically significant ($P > 0.05$) (Mann-Whitney [Wilcoxon] test).

The Calculation of End-plate Potentials

To simulate the end-plate potentials (EPP), the cable equation was solved including Eq. 2 in the first seven segments of the cable. ϕ_1 and ϕ_2 were set as 0.076 and 0.038 NTU respectively, to mimic the experimental estimates of the EPC kinetics at resting membrane potential (Takeuchi and Takeuchi, 1959). The membrane potential of the first segment of the cable is presented in Fig. 3. The values of the time constants used in the calculation of the EPP in Fig. 3 were used throughout the work described in this communication.

The Calculation of Basal Control Currents

To calculate the control current, the steady-state potential profile along the cable was initially estimated by the Euler procedure. The Euler algorithm was applied "backwards," starting the integration at a point far enough for the membrane current-voltage relation to be linear. With this initial condition the integration proceeded towards the origin (Jack et al., 1975; Arispe and Moore, 1979). To decrease the difference between the membrane potential of adjacent segments depolarized by clamping beyond 60 mV, δx was set to 10 μm for the Euler integration. Because the implicit Crank-Nicholson-Forsythe-Wasow (CNFW) procedure was carried out in steps of 20 μm, the Euler profile was shifted along the x axis to equate the potential of the first segment of the cable with the proper segment of the profile. The potential of the remaining segments of the cable was then matched sequentially with the potential of the second segment of the profile, and the voltage-dependent parameters of the equations initialized accordingly.

The potential profile initialized as indicated, through the Euler integration, was approximately equal to the profile calculated integrating the cable equation with only the CNFW algorithm. Fig. 4 is a plot of control current vs. time. The current at the origin is the control current calculated, as explained in Methods, from the Euler profile. At other times, the control current was determined by means of the implicit integration.

The differences between the Euler and the CNFW

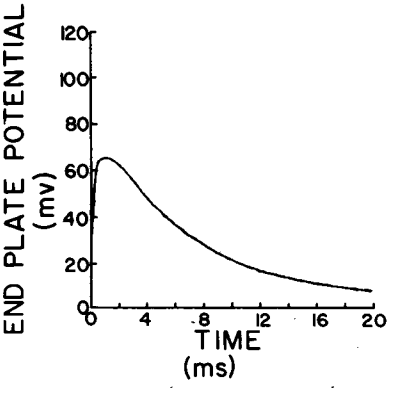

FIGURE 3 Simulation of EPP. The EPP was simulated by means of the cable model with the sodium and potassium conductances in the sarcolemma set equal to zero. $\bar{g}_{Na} = 0$ mS/cm^2, $\bar{g}_K = 0$ mS/cm^2.

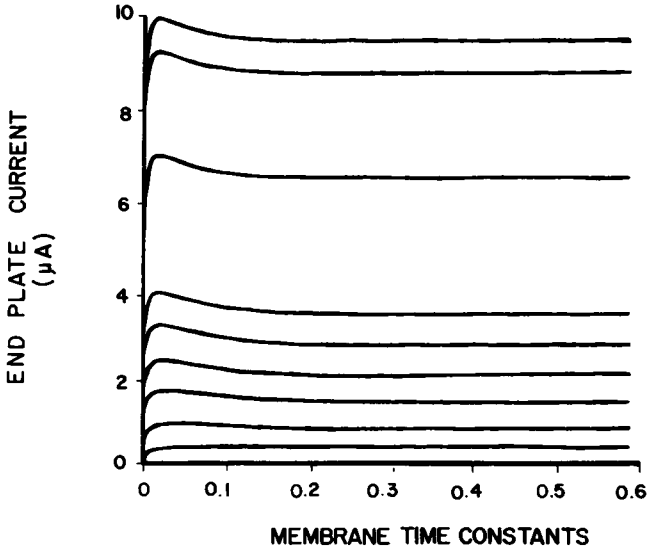

FIGURE 4 Control current calculated clamping the first segment at several membrane potentials. The current was calculated by means of a combination of Euler and the CNFW algorithms (see text). The traces were calculated holding the first segment at (from bottom to top) 50, 60, 70, 80, 90, 100, 140, 170, and 180 mV.

integrations produce some changes during the first 0.18 NTU of the calculated currents. This period is, however, considerably shorter than the time required by the CNFW procedure alone, and because after this time the traces reach steady values (Basal control current) the procedure saves considerable computer time. In all the simulations of EPC presented in this communication, the basal control current was determined after at least 0.3 NTU of stabilization.

Calculation of End-plate Currents

The peak EPC predicted by the nonlinear cable model, is shown in Fig. 5. The figure consists of two plots of current as functions of potential at the control point. The halves of the figure differ in maximum end-plate conductance, decreased from its normal value (1 mS/cm) in Fig. 5*A* to 3% of its value, in Fig. 5*B*. Solid lines indicate the current-voltage (I–V) relation calculated with Eq. 2 assuming perfect control over the synaptic area. The EPC predicted by the point voltage-clamp model differs in magnitude and reversal potential from the current calculated with Eq. 2. Fig. 6 presents similar results, calculated setting the sodium and potassium conductances of the sarcolemma to zero. The end-plate I–V relations in Fig. 6 are linear, although the conductance is overestimated and the apparent reversal potential is more positive than the value used in Eq. 2. Fig. 6*A* also illustrates the effect of reducing fiber diameter from 80 to 50 μm. Paradoxically, the reduction in fiber diameter results in a I–V relation closer to the theoretical one, even though the end-plate parameters were not changed.

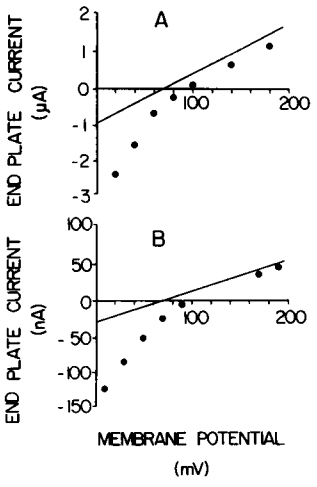

FIGURE 5 End-plate current-voltage (I-V) relation calculated from the cable model with point voltage clamp of the middle of the junction. Dots, current calculated from the cable model; solid lines, I-V relation calculated assuming space clamp of the junction. *A*, normal end-plate conductance (1 mS/cm). *B*, end-plate conductance reduced to 0.03 mS/cm. The ordinate is microamperes in *A* and nanoamperes in *B*. The abscissa in millivolts.

End-plate Currents with Double Voltage Clamp

One possibility to explain the discrepancies between the apparent peak EPC calculated from the point voltage-clamp model and the current predicted by Eq. 2 with perfect control (Figs. 5 and 6) is that the potential profile

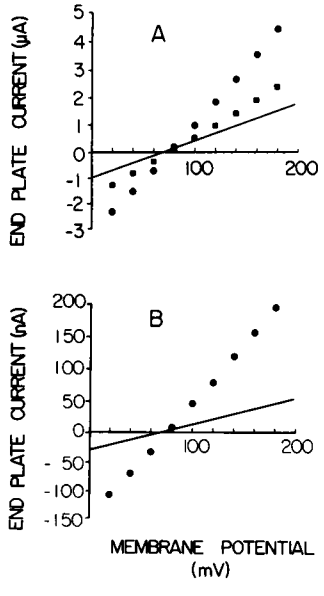

FIGURE 6 The figure presents the I–V relation of the end plate on a linear cable where the sodium and potassium conductances of the sarcolemma were reduced to zero. The other details in the figure are entirely similar to Fig. 5 except for the linearization of the cable and for the I–V relation calculated reducing the fiber diameter from 80 (dots) to 50 μm (squares). (Fig. 5.)

changes during activity, beyond the junctional area, requiring the injection of current in excess of the current needed to control the junction alone.

The former hypothesis was tested simulating a condition where the potential at both ends of the end-plate region is controlled. Because the cable is assumed to be symmetric about the center of the neuromuscular junction, the current needed to control the end plate may be calculated with Eq. 5, changing the subindexes that indicate segment number to give

$$I_{vc} = (V_{7,T} - V_{6,T})/(\delta x\, r_i) + I_{g7,T} + I_{ep7,T}. \qquad (6)$$

The cable was initially assumed isopotential over the whole end-plate area, and then allowed to stabilize with the CNFW algorithm mantaining $V_{7,T}$ constant. The current flowing from the seventh segment to the next does not change after the cable is in a steady state, is a constant part of the basal current, and does not need to be considered for the calculation of EPC.

Fig. 7 shows currents calculated with the double control at the ends of the junction. The currents were calculated with Eq. 6 subtracting the basal current after a stabilization period of 0.3 NTU for plots 7*A* and *B* or 0.6 NTU for 7*C* and *D*. The maximum end-plate conductance was 1 mS/cm for *A* and *B*, and 0.03 mS/cm for *C* and *D*. The value of maximum potassium conductance was 45.5 mS/cm^2 (Adrian and Peachey, 1973) in *A* and *C* and was

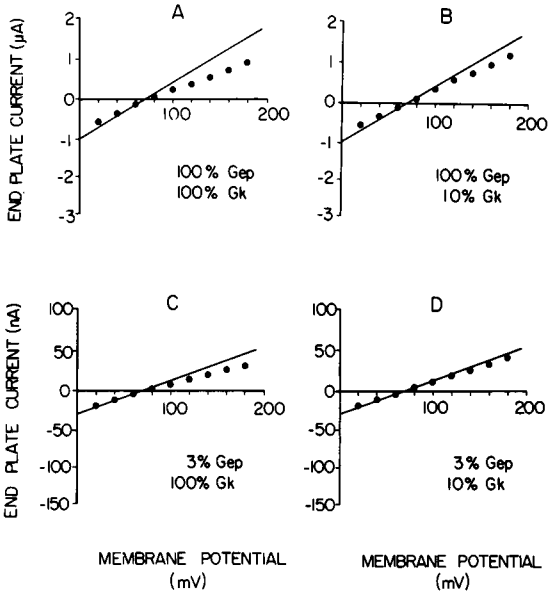

FIGURE 7 End-plate I–V relation calculated from the cable model with double voltage clamp at the extremes of the junction. *A*, normal end-plate and potassium conductances. *B*, normal end-plate conductance and potassium conductance reduced to 4.55 mS/cm (10%). *C*, end-plate conductance reduced to 0.03 mS/cm (3%) and normal potassium conductance. *D*, low end-plate (3%) and potassium (10%) conductances. The ordinate in *A* and *B* is in microamperes and is in nanoamperes in *C* and *D*.

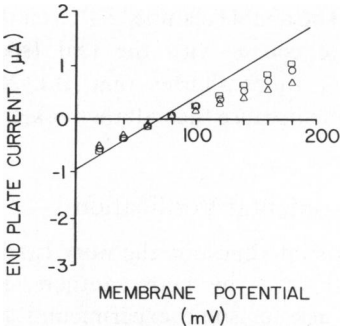

FIGURE 8 Effect of fiber diameter on the endplate I–V relation of double clamped end plates. The figure is similar to Fig. 7*A* in all respects but with three different diameters: Δ = 50, 0 = 80, and □ = 120 μm.

reduced to 10% of this value in *B* and *D*. The figure shows very good fit between the theoretical I–V relation and the current obtained from the cable model with double clamp. The results in 7*D* indicate that the fit between the dots and the line is almost perfect if end plate and potassium conductances are low. All the I–V relations in Fig. 7 were calculated for a fiber of 80 μm in diameter. Fig. 8 is similar to Fig. 7*A* in all aspects except for the fiber diameter. Fig. 8 illustrates that the double clamp approaches the theoretical I–V relation as the diameter increases, as would be expected for the changes in length factor (liberal equivalent of the "length constant" of a linear cable, see for example Arispe and Moore, 1979).

Fig. 9 permits a comparison of the time course of the conductances calculated at the extremes of the voltage range in Figs. 5*A* and 7*A*. The kinetics of apparent end-plate conductance under point clamp depends on membrane potential especially at time > 0.1 NTU. Both EPC represented by solid lines differ in slope with the true

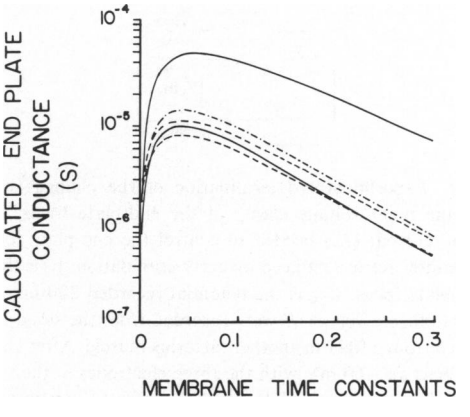

FIGURE 9 Apparent end-plate conductance calculated as function of time. The calculated membrane conductance is presented in logarithmic scale as function of time in normalized time units. Broken-dotted line is the true conductance calculated with the end-plate function and space-clamped end plate. Solid line was calculated from the point voltage-clamp cable model, broken lines from double clamp of the junction. The upper line of each pair was calculated with the control segments held at 180 mV, the lower traces of each pair at 20 mV.

conductance. The double clamped EPC, on the other hand, differs in time course with the real (space clamped) conductance at times shorter than 0.1 NTU, but not beyond this time because then all the broken lines in Fig. 9 are parallel.

Experimental Verification

This paper calls into question the work carried out during more than 20 years by many authors, thus it seems reasonable to ask for some experimental support to our claims. Although precise experimental verification of all the points discussed is probably very difficult if not impossible, the data in Fig. 10 suggest that at least the changes in potential profile in the vicinity of the end plate indicated in Fig. 11 are close to what really happens. In spite of some differences between the two fibers shown in the figure, the change in V_{200} in both of them is in excellent agreement with the data in Fig. 11, and the changes are not due to interelectrode capacitive coupling (Fig. 10*B*). Given that neuromuscular transmission was not inhibited by any treatment in the fibers shown in the figure, EPC are relatively high, but still lower than the ones predicted by the model (see Fig. 5*A*). End plates with currents >1 μA were observed, but are not shown because the control was not good.

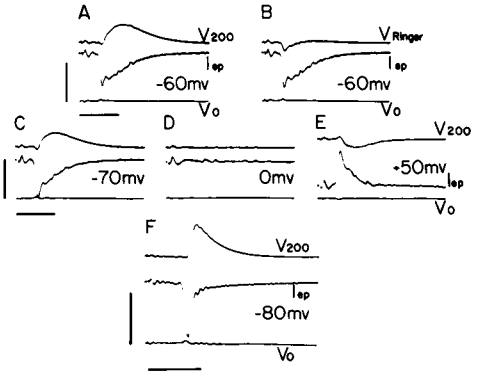

FIGURE 10 Experimental determination of the changes in potential profile during point voltage clamp of the end-plate focus. The figure presents the current (I_{ep}) needed to control the end-plate focus during neurotransmitter release induced by nerve stimulation. V_0 is the potential at the end-plate focus. V_{200} is the potential recorded 200 μm away from the end-plate focus. Sets *A–E* were recorded from the same fiber and *F* was recorded from a fiber in another sartorius muscle. After clamping the end-plate focus at −60 mV with the three electrodes in their places (*A*) the distant electrode was withdrawn (*B*), reinserted again to the same fiber, and the remaining sets of traces (*C*, *D*, and *E*) recorded. The resting potential of both fibers in this figure was −85 mV before the insertion of the current and distant electrodes, and decreased afterwards to −65 mV in fiber *A–E* and to −70 mV in fiber *F*. The fibers were held at −60 mV (fiber *A–E*) and −80 mV (fiber *F*). The membrane potential indicated on each set was imposed to the focus of the end plate, 1 s before stimulating the nerve, and returned to the original value 0.5 s later. The calibration bars indicate 6 ms for the abscisa, 30 mV for V_{200} and V_{Ringer}, and 12 mV for V_0 in all the sets, but indicate 300 nA for I_{ep} in *A–E*, and 600 nA for I_{ep} in *F*. No neuromuscular transmission blocker was used.

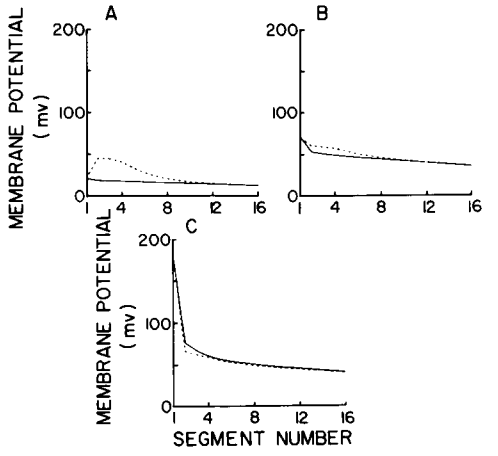

FIGURE 11 Potential profile along the first 16 segments of the cable. Point voltage clamp. Solid lines indicate membrane potential before activating the end-plate function. For this figure in particular the fiber diameter was reduced to 50 μm, the end-plate function was placed in the first 4 segments of the cable divided into 200 segments of 50 μm in length. Broken lines are the membrane potential calculated when the EPC reaches its maximum value. *A*, first segment held at 20 mV. *B*, first segment held at 70 mV (E_{ep}). *C*, first segment held at 180 mV. The potential is drawn at the distal end of each segment.

DISCUSSION

This work analyzes the reliability of the point voltage-clamp technique as applied to the study of end-plate transmission of impulses. For this purpose an empirical end-plate function was devised and placed in the first seven segments of a nonlinear cable that represented the muscle fiber.

The end-plate function used is completely empirical and, in devising this function, we have only tried to reproduce the degree of shunt produced by the neuromuscular junction in frog muscle (Fatt and Katz, 1951). ϕ_1 and ϕ_2 were selected in such a way that the EPC predicted by Eq. 2 resembles the kinetics of the EPC in frog muscle at resting potential. In addition, E_{ep} was chosen to match the reversal potential of the EPC extrapolated from the results of Takeuchi and Takeuchi (1959), 70 mV in our membrane coordinates. Because an extensive search of the literature failed to reveal quantitative evidence on the longitude of the frog muscle fibers occupied by the nerve terminal, especially as a function of fiber diameter, this relation was determined experimentally in frog muscle fibers. The median values of fiber diameter and end-plate length were found to be 80 and 382 μm respectively. Because this work stemmed from a critical attitude towards the point voltage-clamp technique as applied to end plates, we decided to give some bias in favor of this technique by using 80 μm as the diameter of the cable in the model, and 260 μm as the length of the end plate (seven segments of 20 μm simulated plus six segments in the other, symmetric, side of the junction). The regression line in Fig. 2 indicates that a 260 μm junction is likely to exist in a fiber of 44 μm diameter.

Our results indicate that the lack of a space clamp in the voltage-clamp studies of the frog neuromuscular junction produces incorrect estimates of the end-plate properties, even when the conductance is reduced >30 times its normal value. The cable properties of the muscle fiber are able to cause a severe distortion of the point voltage-clamp estimates of the end-plate function. Figs. 5 and 6 suggest that the non-ohmic sodium and potassium conductances of the sarcolemma are able to introduce nonlinearities in the apparent I–V relation of the end plate observed in Fig. 5. Several features of Figs. 5 and 6, however, need some explanation. First, the reversal potential of EPC estimated from the cable model is more positive than the real value, and this difference slightly increases (Fig. 5) when the end-plate conductance is reduced. This and several other findings may be better understood if the behavior of the potential profile of the cable and its changes during end-plate activity are considered. For economy of computer time and memory this was done in a 200 segment cable of 50 μm per segment, with the end plate in the first four segments, and solved for 50 μs time increments. The membrane potential of the initial 16 segments of this cable model, with the first segment clamped at either 20, 70, or 180 mV, is shown in Fig. 11. The solid lines indicate the potential profile before activation of the end-plate function; broken lines are the same profile at the moment when the EPC reaches its maximum value. As may be appreciated in the figure, clamping the potential of the first segment does not prevent changes in the potential of the remaining segments of the cable. When the end plate is active the membrane potential of the end-plate area and its vicinity shifts towards E_{ep} and only the first (clamped) segment remains fixed; this shift in potential profile will propagate farther away from the junction area as the fiber diameter gets bigger. The greater discrepancies between the reversal potential of EPC calculated from the cable model and from the space-clamped end-plate function when $\hat{g}_{ep}$ is reduced are produced by the change of the potential profile during the activation of the conductance. The shift of the membrane towards E_{ep} during end-plate activity improves the space clamp when the center of the neuromuscular junction is held close to E_{ep} and thus a smaller difference is observed between this potential and the reversal of the apparent EPC. When $\hat{g}_{ep}$ is decreased, the potential profile changes less during activity of the neuro-muscular junction, and, as result, the segment under control will have to be driven to more positive values to reverse the apparent EPC. More precisely, because in the discrete cable model at any time

$$I_{ep} = g_{ep} \sum_{i=1}^{n} (V_i - E_{ep}) \qquad (7)$$

with $g_{ep} = \hat{g}_{ep}\, \delta x$ it may be shown that when $I_{ep} = 0$

$$\Delta E_{ep} = V_1 - E_{ep} = (n-1)\, E_{ep} - \sum_{i=2}^{n} V_i \qquad (8)$$

will tend to zero as $\sum_{i=2}^{n} V_i$ approaches $(n-1)\, E_{ep}$, that is when the end plate is space clamped and V_1 is at E_{ep}.

The second feature in Fig. 5 that must be explained is that EPC calculated from the cable model is more negative than the current predicted by Eq. 2 for the space clamped junction. This is prominent at potentials more positive than E_{ep}, and the discrepancy when scaled is about the same with normal (Fig. 5*A*) and reduced g_{ep} (Fig. 5*B*). The I–V relation calculated from the cable model is also markedly nonlinear. The data in Fig. 6, indicate that the nonlinear shape of the I–V relation calculated from the cable in Fig. 5 is produced by the non-ohmic sodium and potassium conductances of the muscle membrane. However, the I–V relations (dots) in Fig. 6 still show a reversal potential more positive than the one of the solid lines, and both halves of the figure coincide in that the end-plate conductance is overestimated by the point clamp technique. Both types of error decrease when fiber diameter diminishes from 80 to 50 μm. Given that the length factor increases with the square root of the diameter, the better fit between the solid lines and the squares suggest that the overestimation of g_{ep} from the I–V relations in Fig. 6 and at the more positive potentials in Fig. 5, reflects additional current injected at the control point to partially clamp changes of potential profile beyond the end-plate area. This is also supported by the results with double voltage clamp in Fig. 8. The removal of the voltage changes during end-plate activity outside of the junctional area reduces the effect of diameter on the I–V relation, and the current predicted from the double-clamp cable model approaches the ideal current as the diameter gets larger, as expected from linear cable theory. This is illustrated in Fig. 8 for the worst case: maximum end-plate conductances without potassium inactivation.

This paper also presents theoretical evidence suggesting that it is possible to voltage clamp end plates in frog sartorius muscle with little error, if the membrane potential is controlled at both ends of the junction. The I–V relations calculated from the cable model in Fig. 7*A* and *C*, in conditions of maximum nonlinearity, are better approximations to the space-clamped end plate than any of the I–V relations in Figs. 5 or 6. The error with the double clamp is largest at depolarizations between 100 and 200 mV, but this diminishes if the potassium conductance of the sarcolemma is decreased from 45.5 mS/cm^2 to 10% of this value. The almost perfect fit between the double-clamped and space-clamped EPC in Fig. 7*D* is noteworthy because the conditions simulated are feasible in real life. The low end-plate conductance corresponds to curarized neuromuscular junctions or to EPP with their quantal content depressed, and the low potassium conductance is similar to the value observed after g_K inactivates during a long depolarizing pulse (Adrian et al., 1970).

From the results discussed, it is apparent that the point voltage-clamp technique of frog neuromuscular junctions is quantitatively unreliable. The results calculated with a

relatively short "curarized" end plate (Fig. 6*B*) on a completely voltage independent (Fig. 6) fiber of average diameter overestimates the junctional conductance by close to 4 times. That is, 75% of the current injected at the control point flows through nonjunctional membrane, and this seems unavoidable as long as just two microelectrodes are used to clamp the end plate, unless the junction is placed on an unusually short fiber. Separating the current and voltage sensing electrodes is not likely to help much. If the current electrode is in the middle of the junction and the voltage-sensing electrode is at one of its ends, this half of the junction will resemble the double clamp. The other half, however, will be free to fluctuate at least as much as any of the halves with both electrodes in the middle of the end plate, and perhaps more. Thus the results obtained, in the best of circumstances, will lie between those obtained with point and double voltage clamp. Although the results in this paper indicate that the magnitude, kinetics, and reversal potential of EPC are in error when the point voltage clamp is used, the worst disparity occurs in the magnitude of the conductance estimates. For each microampere of control current flowing through the junction, 2 or 3 μA flow through nonjunctional membrane. From our results it is difficult to predict what is the effect of the lack of space clamp on electric noise from acetylcholine-sensitive channels, or the amount of error when end plates other than frog's are clamped. It would seem wise, though, to be cautious with the quantitative analysis of any parameter obtained with point voltage clamp of end plates. The double-clamp condition simulated here is very promising and, although it has not been tried in practice, it could perhaps be achieved with some sort of clamp with four microelectrodes, two to pass current and two to sense voltage, one of each kind at each end of the junction. Another possibility may be some kind of double-gap voltage clamp with the end plate in between.

We would like to express our kindest appreciation to Dr. Carlo Caputo for critically reading the manuscript and providing the voltage clamp circuit, to Miss I. Otaegui and Mrs. L. Sevcik for their secretarial assistance, and to Mrs. Mary Sguazzin for proof reading the manuscript.

The PDP-11/10 computer and its peripherals were financed by grants No. 31.26. S1-0590 and S1-0754 from the Venezuelan Consejo Nacional de Investigaciones Científicas y Tecnológicas. The PDP 11/34 was used at the Instituto Venezolano de Investigaciones Científicas computer center.

Received for publication 21 March 1980 and in revised form 8 December 1981.

REFERENCES

Adrian, R. H., W. K. Chandler, and A. L. Hodgkin. 1970. Voltage clamp experiments in striated muscle fibers. *J. Physiol.* (Lond.). 208:607–644.

Adrian, R. H., and L. D. Peachey. 1973. Reconstruction of the action potential of frog sartorius muscle. *J. Physiol. (Lond.).* 235:103–131.

Arispe, N. J. 1972. The cable properties of a nonlinear axon. Ph.D. Dissertation. Department of Physiology and Pharmacology, Duke University Medical Center, Durham, NC.

Arispe, N. J., and J. W. Moore. 1979. Nonlinear cable equations for axons. I. Computations and experiments with internal current injection. *J. Gen. Physiol.* 73:725–735.

Crank, J., and P. Nicholson. 1947. A practical method for numerical evaluation of solutions of partial differential equations of heat conduction type. *Proc. Cambridge Phyl. Soc.* 43:50–67.

Fatt, P., and B. Katz. 1951. An analysis of end-plate potential recorded with an intra-cellular electrode. *J. Physiol. (Lond.).* 115:320–370.

Forsythe, G. E., and W. R. Wassow. 1960. Finite-difference Methods for Partial Differential Equations. John Wiley & Sons, Inc., New York. 96.

Hodgkin, A. L., and W. A. Rushton. 1946. The electrical constants of crustacean nerve fiber. *Proc. Royal Soc. Ser. B.* 133:444–479.

Hodgkin, A. L., A. F. Huxley, and B. Katz. 1952. Measurement of current-voltage relations in the membrane of the giant axon of *Loligo. J. Physiol. (Lond.).* 116:424–448.

Hodgkin, A. L., and A. F. Huxley. 1952*a*. Currents carried by sodium and potassium ions through the membrane of the giant axon of *Loligo. J. Physiol. (Lond.).* 116:449–472.

Hodgkin, A. L., and A. F. Huxley. 1952*b*. The components of membrane conductance in the giant axon of *Loligo. J. Physiol. (Lond.).* 116:473–496.

Hodgkin, A. L., and A. F. Huxley. 1952*c*. The dual effect of membrane potential on sodium conductance in the giant axon of *Loligo. J. Physiol. (Lond.).* 116:497–506.

Hodgkin, A. L., and A. F. Huxley. 1952*d*. A quantitative description of membrane current and its application to conduction and excitation in nerve. *J. Physiol. (Lond.).* 117:500–544.

Hollander, M., and P. A. Wolfe. 1973. Nonparametric statistical methods. John Wiley & Sons, Inc., New York. 1–82.

Lack, J., D. Noble, and R. Tsien. 1975. Electric Current Flow in Excitable Cells. Clarendon Press, Oxford.

Kootsey, J. M., and E. A. Johnson. 1972. Voltage clamp of cardiac muscle. A theoretical analysis of early currents in the single sucrose gap. *Biophys. J.* 12:1496–1508.

Kuno, M., S. A. Turkanis, and J. N. Weakly. 1971. Correlation between nerve terminal size and transmitter release at the neuromuscular junction of the frog. *J. Physiol. (Lond.)* 213:545–556.

Löwit, 1875. Die nerven der glatten musculatur. Wiener Stitzber 71. Referred to by B. Romeis. 1968. *Microskopische Technik.* R. Oldenbourg Verlag. Munich. 478

Sevcik, C., and T. Narahashi. 1972. Electrical properties and excitation-contraction coupling in skeletal muscle treated with ethylene glycol. *J. Gen. Physiol.* 60:221–236.

Takeuchi, A., and N. Takeuchi. 1959. Active phase of frog's endplate potential. *J. Neurophysiol.* 22:395–411.